

A Novel Method for Fault Detection in Future Renewable Electric Energy Delivery and Management Microgrids, Considering Uncertainties in Network Topology

Reza Eslami, Seyed Hossein Hesamedin Sadeghi, Hossein Askarian-Abyaneh & Adel Nasiri

To cite this article: Reza Eslami, Seyed Hossein Hesamedin Sadeghi, Hossein Askarian-Abyaneh & Adel Nasiri (2017) A Novel Method for Fault Detection in Future Renewable Electric Energy Delivery and Management Microgrids, Considering Uncertainties in Network Topology, *Electric Power Components and Systems*, 45:10, 1118-1129, DOI: [10.1080/15325008.2017.1292433](https://doi.org/10.1080/15325008.2017.1292433)

To link to this article: <http://dx.doi.org/10.1080/15325008.2017.1292433>



Published online: 28 Jul 2017.



Submit your article to this journal [↗](#)



View related articles [↗](#)



View Crossmark data [↗](#)

A Novel Method for Fault Detection in Future Renewable Electric Energy Delivery and Management Microgrids, Considering Uncertainties in Network Topology

Reza Eslami,¹ Seyed Hossein Hesamedin Sadeghi,^{1,2} Hossein Askarian-Abyaneh,¹ and Adel Nasiri²

¹Department of Electrical Engineering, Amirkabir University of Technology, Tehran, Iran

²Department of Electrical Engineering, University of Wisconsin-Milwaukee, Milwaukee, Wisconsin, USA

CONTENTS

- 1. Introduction
 - 2. Proposed Method
 - 3. Simulated Results
 - 4. Conclusions
- References

Abstract—The use of solid state transformers (SSTs) in microgrids has created a new kind of network called Future Renewable Electric Energy Delivery and Management (FREEDM) microgrid. The FREEDM microgrid provides an appropriate means for enhanced energy management, loss reduction, and network flexibility by reducing the number of converters used for a variety of AC-DC links. In this work, we propose a novel method for fault detection in FREEDM microgrids when considering uncertainties in network topology. The proposed method makes use of the Clarke and S-transforms to characterize the transients in three-phase current and voltage waveforms in the event of a fault. The extracted features of the waveforms will be used to form appropriate indices for detection, location, and characterization of the fault. The main feature of the proposed method is its capability to operate in a dynamic microgrid with varying topology. The performance of the proposed method is investigated by applying it to a sample FREEDM microgrid with ring and radial structures. It is shown that the proposed method is well capable of fault detection and diagnosis while being able to differentiate between short-circuit faults and switching transients due to variations in the network topology.

1. INTRODUCTION

Solid state transformer (SST) is a transformer relevant to power electronic devices that are introduced with the advancement of semi-conductor technology. It comprises high-powered semiconductor components, conventional high-frequency transformers, and control circuitry to form a flexible means for controlling power distribution networks [1]. Due to special properties of these transformers (such as bi-directional power flow and input/output AC/DC power availability), they are gradually replacing the conventional transformers in intelligent networks [2].

The presence of SSTs in microgrids has created a new class of smart networks called Future Renewable Electric

Keywords: FREEDM microgrid, fault detection, S-transform, Clarke components, signal energy

Received 29 May 2016; accepted 23 January 2017

Address correspondence to Seyed Hossein Hesamedin Sadeghi, Department of Electrical Engineering, Amirkabir University of Technology, 424 Hafez Ave., Tehran 15914, Iran. E-mail: sadeghi@aut.ac.ir

Energy Delivery and Management (FREEDM) microgrids. The FREEDM microgrid provides an appropriate means for energy management, loss reduction, and network flexibility by reducing the number of converters used for a variety of AC-DC links [3]. These merits are welcomed by many policy-makers who believe a smart grid is not only needed to remedy the problems caused by the grid's growth in size, scale, and complexity, but is well within reach.

Similar to the conventional microgrids, the protection of FREEDM networks in the event of a short-circuit fault is a challenging task. In this endeavor, fault detection is found to be the main challenge due to the low magnitude of fault current in the presence of inverter-interfaced distributed generations (IIDGs). To overcome this issue, the installation of synchronous DGs in the vicinity of IIDGs has been proposed for balancing out the fault current [4]. The proposed scheme, however, becomes increasingly complicated when the dynamic behavior of microgrids is taken into account, let alone the undesirable economic burden it could impose [5].

A thorough review of various fault detection methods in the conventional microgrids has been reported in [5]. These methods include voltage analysis, wavelet transform, S-transform (ST), and harmonic analysis. In the voltage analysis method, the output voltages of DGs [6, 7], or their transformed values in the d-q axes [8], are compared with appropriate threshold values. This method cannot be applied to all microgrid topologies as the threshold values are dependent on the topology of the microgrid. In the wavelet transform method, a decision-maker tree is generated based on a number of components extracted from distorted voltage and current waveforms in the event of a fault [9]. Although this method is applicable to networks with known topologies, it fails to detect faults in a typical microgrid with uncertainties in its topology. In the ST method, a constant threshold value is used for detecting a fault [10]. Again, it tends to fail as the use of a constant threshold value cannot guarantee accurate fault detection in all possible network topologies. In the harmonic analysis method, the zero component of current waveform is used for fault detection. Therefore, it can only detect phase-to-ground faults, missing the other types of faults in the network [11]. In a different approach, digital relays have been used to monitor current differential for fault detection [12–16]. This approach can only cover the normal and island modes of operation and is incapable of treating all microgrid topology variations.

Despite various techniques mentioned above for detection of faults in the conventional microgrids, there are few reports in the literature that involve FREEDM microgrids. Fault detection in FREEDM systems generally involves more complex challenges, partly due to the presence of SSTs. It

is worth noting that the high-frequency isolation in a SST strongly decouples its two sides in a way that distorted signals in either side are not observed in the opposite side [17, 18]. The authors in [18, 19] proposed the central-adaptive protection method for fault detection in a FREEDM system. In this method, the microgrid ring is divided into several zones whereby the fault detection is done based on current differential in each zone. If the sum of the currents inside each zone is equal to zero, there is no fault in that zone; otherwise, fault exists and a cut off command will be sent to the breakers at the end points of each zone. The use of adaptive schemes for protection of microgrids equipped with power electronics devices was challenged due to the problems in the synchronizing measurements and data transfer [3, 20]. The issue was resolved using the inherent attributes of SSTs.

None of the above-mentioned methods considers the uncertainties in the topology of a FREEDM system. In this paper, we propose a novel method for detection of faults in a FREEDM microgrid. The proposed method makes use of the Clarke transform and ST to obtain the characteristics of three-phase current and voltage waveforms and their Clarke components at different points in the network. The information is used to detect fault occurrence, fault location, fault type, and the respective engaged phases. The ST provides a high-resolution mapping of transient signals in the frequency domain, using frequency-variable Gaussian windows [21]. This feature enables one to have access to very useful time-domain information about transient signals which, in turn, can be used to determine various characteristics of a fault while differentiating it from switching of energy sources, loads, or network lines.

One of the innovations in the proposed method is its capability to respond to varying topology of a dynamic microgrid. In fact, there is no need to change the protection strategy in the proposed method in cases where the microgrid utilization topology changes. Also, it is independent of the inherent properties of SST so that the forced complexities for the microgrid due to the presence of these transformers do not affect the effective performance of the proposed method.

The paper is structured as follows. In Section II, the proposed method is detailed and an algorithm for implementation will be introduced. The sample microgrid is described in Section III where simulated results of various case studies are presented to evaluate the performance of the proposed method for both ring and radial topologies.

2. PROPOSED METHOD

Without loss of generality, we assume that the FREEDM microgrid (Figure 1) has a ring structure and is divided into

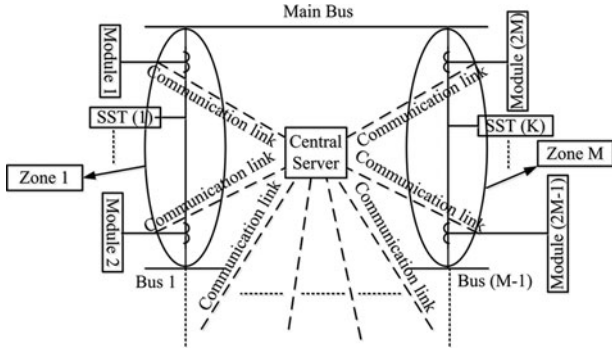


FIGURE 1. The main ring of a typical FREEDM microgrid system.

M zones. We also assume that the m -th zone ($m = 1: M$) comprises two sensing modules at its two ends for capturing current and voltage waveforms. The captured data are sent to a central server through appropriate communication links, where it determines the occurrence of a fault, its type, and the zone within which it occurs [22]. For the sake of simplicity, we assume that the communication links as well as sensing modules are noise-free.

2.1. Clarke Transform

When a fault occurs, the three-phase current and voltage waveforms will vary everywhere in the network, particularly in the vicinity of the fault location. The analysis of such variations can be used to determine the type of a fault and its location [23]. Considering that the zero components of the current and voltage waveforms in the event of a fault are no longer zero, we start by applying the Clarke transform to the respective waveforms, *i.e.*,

$$\begin{pmatrix} u_{\alpha}^m \\ u_{\beta}^m \\ u_{\gamma}^m \end{pmatrix} = \frac{1}{3} \begin{pmatrix} 2 & -1 & -1 \\ 0 & \sqrt{3} & -\sqrt{3} \\ 1 & 1 & 1 \end{pmatrix} \begin{pmatrix} u_a^m \\ u_b^m \\ u_c^m \end{pmatrix} \quad (1)$$

where u_{α}^m , u_{β}^m , and u_{γ}^m , respectively, represent the α -, β -, and γ -components of the Clarke transform of the phase a , u_a^m , phase b , u_b^m , and phase c , u_c^m , of the current/voltage waveforms in the m -th module ($m = 1: 2M$).

2.2. S-Transform (ST)

ST is a time-frequency distribution with the attributes of the wavelet transform and the short time Fourier transform simultaneously. It provides a high-resolution mapping of transient signals in the frequency domain, using frequency-variable Gaussian windows [21]. It has been shown that the ST is a powerful tool for voltage and current signal processing with the capability of differentiating a short-circuit fault from

switching transients due to variations in the network topology in a microgrid [24].

The ST, $S(t, f)$, of a time-domain signal, $u(t)$, is defined as follows [21],

$$S(t, f) = \int_{-\infty}^{\infty} u(\tau) \cdot \omega(\tau - t, f) \cdot \exp(-j2\pi f\tau) d\tau \quad (2)$$

where ω is a running Gaussian function window in time whose standard deviation is equal to the reciprocal of frequency ($1/f$), *i.e.*,

$$\omega(\tau - t, f) = \frac{f}{\sqrt{2\pi}} \exp\left(-\frac{(\tau - t)^2 f^2}{2}\right) \quad (3)$$

such that

$$\int_{-\infty}^{\infty} \omega(\tau - t, f) d\tau = 1 \quad (4)$$

It is worth noting that since the maximum magnitude of Gaussian function equals its mean value, the mean value of the window is appointed on the intended moment of the signal to provide more focus on the examined signal.

Assuming that the received signal $u(t)$ is sampled with time interval T and total sampling number N , we get a discrete sequence of $u(k)$, $k = 1, 2, \dots, N$. By defining $f \rightarrow \frac{n}{NT}$ and $\tau \rightarrow kT$, the discrete ST expression can be written as follows,

$$S_{u,q}^m \left[lT, \frac{n}{NT} \right] = \sum_{k=1}^N u_q^m(kT) \cdot \omega \left((k-l)T, \frac{n}{NT} \right) \cdot \exp \left(\frac{-j2\pi kn}{N} \right) \quad (5)$$

where $m = 1: 2M$, $q = \alpha, \beta, \gamma, a, b, c$, and $u = i, v$ represents the current, i , and voltage, v , waveforms.

The result of ST is a duplicate time-frequency $N \times N$ matrix known as the S-matrix; its row vector reflects the frequency distribution of the interval time T , and its column vector reflects the changes of a certain frequency with time.

The S-matrix of signal u_q^m , $S_{u,q}^m$, can be expressed as follows:

$$S_{u,q}^m \left[lT, \frac{n}{NT} \right] = \begin{pmatrix} S_{u,q}^m \left[T, \frac{1}{NT} \right] & S_{u,q}^m \left[T, \frac{2}{NT} \right] & S_{u,q}^m \left[T, \frac{3}{NT} \right] & \cdots & S_{u,q}^m \left[T, \frac{1}{T} \right] \\ S_{u,q}^m \left[2T, \frac{1}{NT} \right] & S_{u,q}^m \left[2T, \frac{2}{NT} \right] & S_{u,q}^m \left[2T, \frac{3}{NT} \right] & \cdots & S_{u,q}^m \left[2T, \frac{1}{T} \right] \\ S_{u,q}^m \left[3T, \frac{1}{NT} \right] & S_{u,q}^m \left[3T, \frac{2}{NT} \right] & S_{u,q}^m \left[3T, \frac{3}{NT} \right] & \cdots & S_{u,q}^m \left[3T, \frac{1}{T} \right] \\ \vdots & \vdots & \vdots & \vdots & \vdots \\ S_{u,q}^m \left[NT, \frac{1}{NT} \right] & S_{u,q}^m \left[NT, \frac{2}{NT} \right] & S_{u,q}^m \left[NT, \frac{3}{NT} \right] & \cdots & S_{u,q}^m \left[NT, \frac{1}{T} \right] \end{pmatrix} \quad (6)$$

from which the energy matrix, $\mathbf{E}_{u,q}^m$, whose elements are the square of the amplitude of the respective elements in the S-matrix, is derived, *i.e.*,

$$\mathbf{E}_{u,q}^m = \begin{pmatrix} |S_{u,q}^m [T, \frac{1}{NT}]|^2 & |S_{u,q}^m [T, \frac{2}{NT}]|^2 & |S_{u,q}^m [T, \frac{3}{NT}]|^2 & \dots & |S_{u,q}^m [T, \frac{1}{T}]|^2 \\ |S_{u,q}^m [2T, \frac{1}{NT}]|^2 & |S_{u,q}^m [2T, \frac{2}{NT}]|^2 & |S_{u,q}^m [2T, \frac{3}{NT}]|^2 & \dots & |S_{u,q}^m [2T, \frac{1}{T}]|^2 \\ |S_{u,q}^m [3T, \frac{1}{NT}]|^2 & |S_{u,q}^m [3T, \frac{2}{NT}]|^2 & |S_{u,q}^m [3T, \frac{3}{NT}]|^2 & \dots & |S_{u,q}^m [3T, \frac{1}{T}]|^2 \\ \vdots & \vdots & \vdots & \vdots & \vdots \\ |S_{u,q}^m [NT, \frac{1}{NT}]|^2 & |S_{u,q}^m [NT, \frac{2}{NT}]|^2 & |S_{u,q}^m [NT, \frac{3}{NT}]|^2 & \dots & |S_{u,q}^m [NT, \frac{1}{T}]|^2 \end{pmatrix} \quad (7)$$

The energy of u_q^m , $E_{u,q}^m$, can now be obtained by summing up the elements of the energy matrix, *i.e.*,

$$E_{u,q}^m = \sum_{e=1}^N \sum_{g=1}^N \left| S_{u,q}^m \left[eT, \frac{g}{NT} \right] \right|^2 \quad (8)$$

and the standard deviation of $\mathbf{E}_{u,q}^m$, $STD_{u,q}^m$,

$$STD_{u,q}^m = \sqrt{\frac{\sum_{e=1}^N \sum_{g=1}^N \left(\left| S_{u,q}^m \left[eT, \frac{g}{NT} \right] \right|^2 - \left(\frac{\sum_{e=1}^N \sum_{g=1}^N |S_{u,q}^m [eT, \frac{g}{NT}]|^2}{N^2} \right)^2 \right)}{N^2}} \quad (9)$$

is computed to examine how much the elements of the energy matrix differ from each other.

We will use values of $E_{u,q}^m$ and $STD_{u,q}^m$ ($m = 1: 2M$, $q = \alpha, \beta, \gamma, a, b, c$, and $u = i, v$) to detect, locate and characterize a fault. Notice that when a fault occurs, various elements of the energy matrix that contain the signal energy at different times and frequencies are altered remarkably; such variations will lead to changes in the values of the examined signal energy and standard deviation of the respective energy matrix. For the sake of consistency, these values are normalized to the largest value which is recorded. Throughout the manuscript, the bar sign ($\bar{}$) is used to indicate the normalized version of the respective quantity.

2.3. Proposed Fault Detection Method

Figure 2 shows a block diagram of the proposed method for determining the occurrence of a fault, its type, and the zone within which it occurs in a FREEDM microgrid. In the proposed method, the central server shares data from various sensing modules with three main algorithms (namely, fault detection, fault location, and fault characterization), each of which is responsible for performing a particular task. A detailed description of each algorithm is given below.

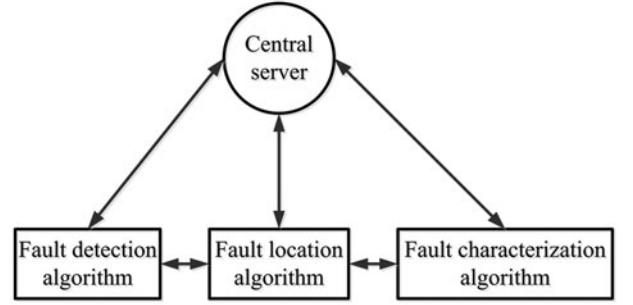


FIGURE 2. Block diagram of the proposed method.

In the fault detection algorithm, the occurrence of a fault in the network is decided by examining the energy and standard deviation of the α - and γ -components of current and voltage energy matrices associated with various sensing modules (Figure 3) against appropriate pre-specified threshold values. The threshold values are obtained off-line, prior to the implementation of the detecting algorithm. This is done by simulating various transients in the network and computing the respective detection indices. In particular, borderline cases (faults with small values of detection indices or non-fault transient disturbances with large values of detection indices) are selected on the basis that the proposed method should be able to detect all genuine faults while not acting on other transient disturbances. To avoid false detection, the threshold value associated with each detection index is determined such that it becomes greater than the largest value of the respective index for non-fault transients while being smaller than those obtained for the faults with smallest impact at the sensing positions (*i.e.*, locating electrically distant from the sensors). In the case where there is not a large gap between the values of a detection index for fault and non-fault transients, a compromise is made and the threshold value is selected to be as close as possible to both values. It is worth noting that a decision for declaring a fault is only made when all four detection indices are greater than the respective thresholds, thus minimizing the chance of a false signal. Also, the use of the ST provides an excellent tool for differentiating between short-circuit faults and switching transients due to variations in the network topology. Hence, one does not expect to see too much changes in the gaps between the threshold values associated with the fault and non-fault transients in the cases where the network topology varies. In other words, variations in the network topology have little effect on the accuracy of the proposed method.

It is worth noting that the standard deviations of transient signals are used to detect the occurrence of a transient disturbance in the network, whereas their energy values are used

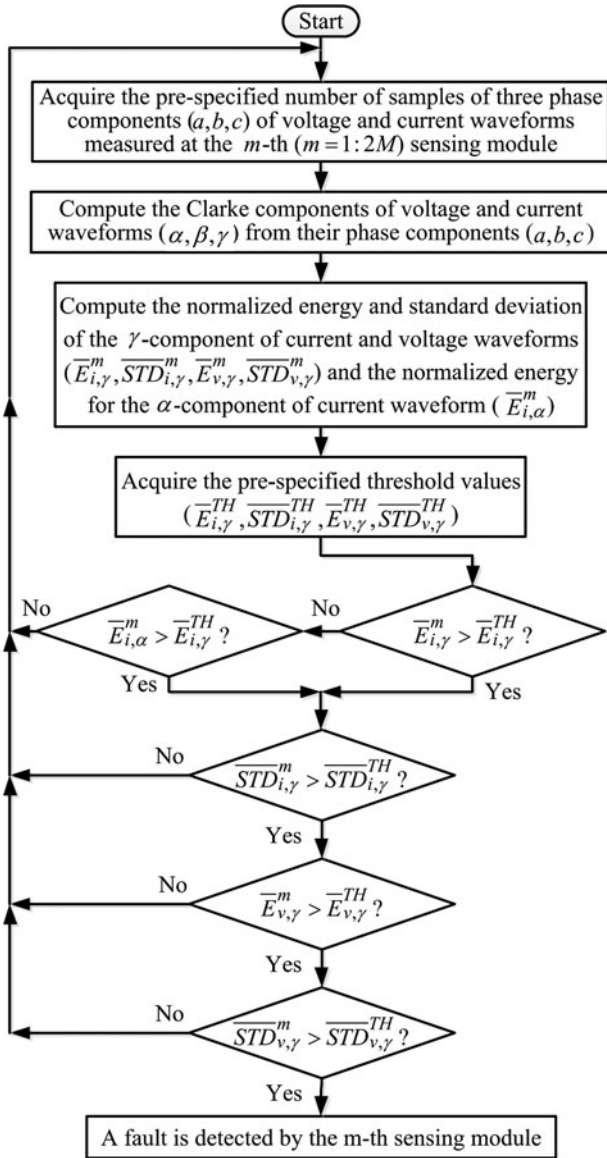


FIGURE 3. Flowchart of the fault detection algorithm.

to differentiate between a short-circuit fault and other cases of transient states (e.g., switching of DGs, loads, or network lines). When the values of all four detection indices (Figure 3) in a sensing module exceed their respective thresholds, the algorithm detects a fault.

Due to the short length of lines in a typical microgrid network, several modules (say L modules) could simultaneously detect a fault; hence, it is important to prevent unreasonable power outages by detecting the exact location of a fault. The fault location algorithm (Figure 4) uses the energy values of the α - and γ -components of current waveforms measured at the L detecting modules to compute the $L \times 1$ location

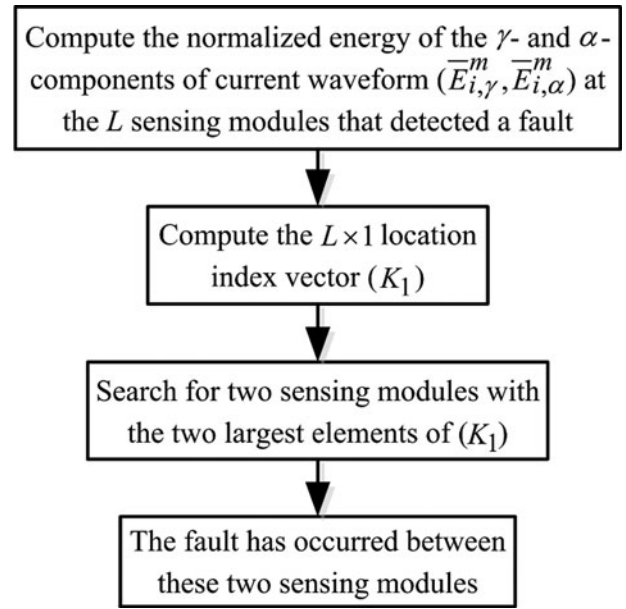


FIGURE 4. Flowchart of the fault location algorithm.

vector, K_1 , defined as follows,

$$K_1 = \begin{bmatrix} \bar{E}_{i,\gamma}^1 + \bar{E}_{i,\alpha}^1 \\ \bar{E}_{i,\gamma}^2 + \bar{E}_{i,\alpha}^2 \\ \bar{E}_{i,\gamma}^3 + \bar{E}_{i,\alpha}^3 \\ \vdots \\ \bar{E}_{i,\gamma}^L + \bar{E}_{i,\alpha}^L \end{bmatrix} \quad (10)$$

Having determined the location index vector, the location algorithm searches for the two sensing modules associated with the two largest elements of the location index vector. The connecting line between these modules is where the fault has occurred.

After locating the position of a fault, the characterizations algorithm (Figure 5) uses the values of energy associated with the α -, β -, and γ -components of current and voltage waveforms of the sensing module ($m = m'$) with the largest detection index to determine the fault type and the corresponding phases. This is done by computing two empirical characterization indices, $K_2^{m'}$ and $K_3^{m'}$, as follows

$$K_2^{m'} = \bar{E}_{i,\gamma}^{m'} + \bar{E}_{v,\gamma}^{m'} \quad (11)$$

$$K_3^{m'} = \max \left\{ (\bar{E}_{i,\alpha}^{m'} + \bar{E}_{v,\alpha}^{m'}), (\bar{E}_{i,\beta}^{m'} + \bar{E}_{v,\beta}^{m'}) \right\} \quad (12)$$

It is found that the values of $K_2^{m'}$ and $K_3^{m'}$ are sensitive to the type of faults, and hence, can be used to characterize a

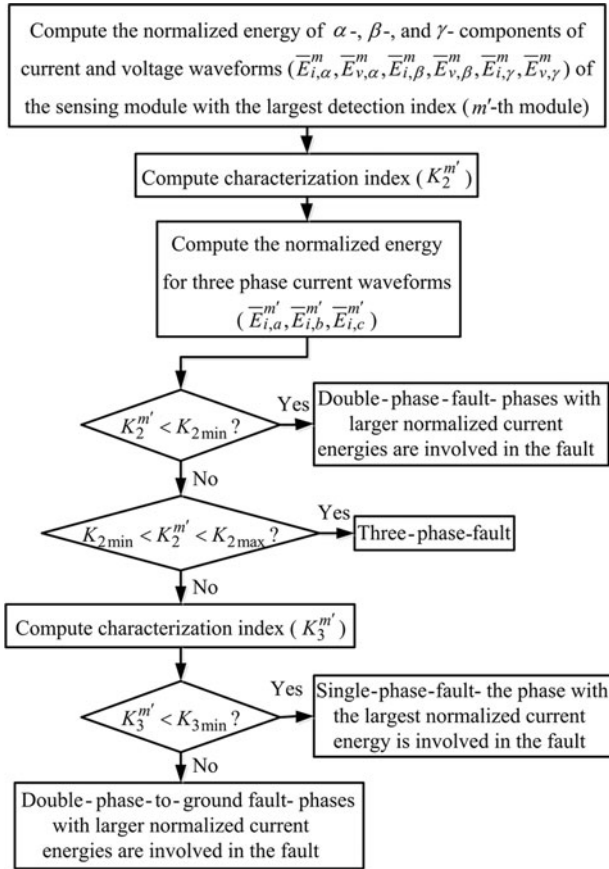


FIGURE 5. Flowchart of the fault characterizations algorithm.

detected fault as follows,

$$\left\{ \begin{array}{ll} K_2^{m'} < K_{2\min} & \Rightarrow \text{Double - Phase} \\ K_{2\min} < K_2^{m'} < K_{2\max} & \Rightarrow \text{Three - Phase} \\ K_2^{m'} > K_{2\max} \text{ and } K_3^{m'} < K_{3\min} & \Rightarrow \text{Single - Phase} \\ K_2^{m'} > K_{2\max} \text{ and } K_3^{m'} > K_{3\min} & \Rightarrow \text{Double - Phase - to - Ground} \end{array} \right. \quad (13)$$

where $K_{2\min}$, $K_{2\max}$, and $K_{3\min}$ denote the thresholds (domain separators) in the $K_2^{m'}-K_3^{m'}$ space whose values are determined based on the network topology, the fault type, and the energy values of the respective components of voltage and current waveforms.

To determine the faulted phase(s), the characterization algorithm uses the energy values of the a , b , and c phase current waveforms measured at the sensing module with the largest detection index. Knowing that the faulty phases carry much larger currents than the unfaulty ones, it follows that the unfaulty phase in a double-phase or double-phase-to-ground, and the faulty phase in a single-phase fault, can be readily recognized, as shown

It is worth emphasizing that the proposed method, as opposed to the conventional methods [3], is capable of detecting a fault in all operational topologies of a FREEDM microgrid. It can also be readily implemented on a microgrid with decentralized controller. In this case, all modules are equipped with the fault detection, fault location, and fault characterizations algorithms, and will be responsible for the required computation and decision making. In the event of a fault, some of the modules will detect a fault according to the flowchart shown in Figure 3, and subsequently, dispatch appropriate detection alarms as well as their computed detection indices to all other modules. The two modules with the largest values of the fault location index (Figure 4) will declare that the fault has occurred along their connecting line. Between these two modules, the one with a larger fault location index will be responsible for determining the type of fault according to the flowchart shown in Figure 5.

3. SIMULATED RESULTS

In order to evaluate the performance of the proposed method, we used the sample microgrid shown in Figure 6 whose data are available in Table 1. As can be seen in this figure, the entire DG sources and some of the loads are connected to the secondary side of the SST while the others are connected to Buses 1–4.

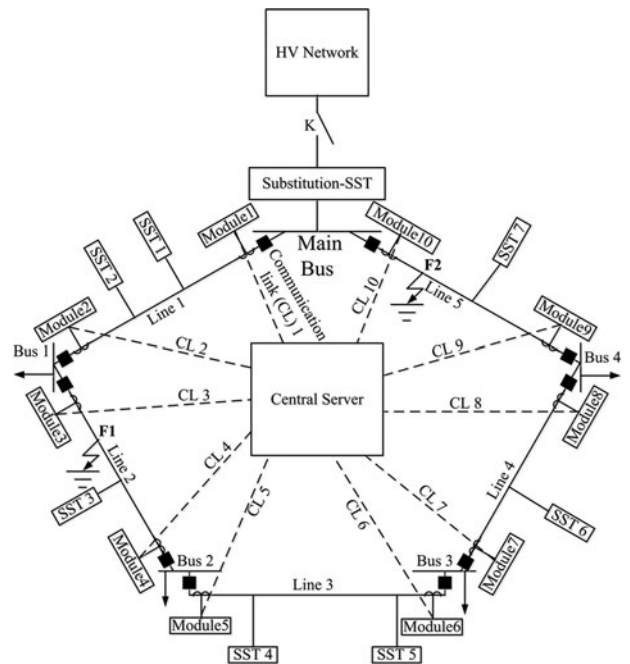


FIGURE 6. Sample FREEDM microgrid.

Lines data		Solid state transformers data							
$R = 0.55 \Omega/\text{km}$		Generation			Load		Bus loads		
$X = 0.3 \Omega/\text{km}$		Name	S(kVA)	PF	S(kVA)	PF	Bus number	S(kVA)	PF
Line 1	2.4 km	SST1	0	0	250	0.8lag	Bus1	330	0.8lag
Line 2	1.3 km	SST2	350	0.9lag	380	0.7lag	Bus2	200	0.9lag
Line 3	3.5 km	SST3	0	0	530	0.9lag	Bus3	250	0.75lag
Line 4	0.9 km	SST4	300	0.9lag	410	0.75lag	Bus4	500	0.85lag
Line 5	1.6 km	SST5	0	0	90	0.85lag			
		SST6	220	0.9lag	430	0.85lag			
		SST7	0	0	260	0.8lag			

TABLE 1. Network data for the 12-kV FREEDM microgrid shown in Figure 6

We use the well-known DIGSILENT Power Factory 14.1.3 for obtaining the simulated results. In all simulations, the proposed method analyzes the voltage and current waveforms of a 100-millisecond sliding window sampled at a rate of 10 kHz. Also, all possible fault types in various locations of the microgrid are simulated and the values of K_{2min} , K_{2max} , and K_{3min} are found to be 0.1, 1, and 1, respectively.

3.1. Detection of a Symmetric Fault

To assess the capability of the proposed method in detection of symmetric faults, a three-phase fault with 200 ohms of fault resistance is placed at point *F1* on Line 2 in the main ring of the sample microgrid, as shown in Figure 6. In order to determine the threshold values similar to those presented in [23, 24], the worst situations that could challenge the proposed method are considered. These situations are chosen on the basis that the proposed method should be able to detect all possible faults while ignoring all transient states. The normalized threshold values associated with the energy and standard deviation of the γ -components of current and

voltage waveforms, $\overline{E}_{i,\gamma}^{TH}$, $\overline{STD}_{i,\gamma}^{TH}$, $\overline{E}_{v,\gamma}^{TH}$, and $\overline{STD}_{v,\gamma}^{TH}$ are found to be 0.000449, 0.001078, 0.002129, and 0.006575, respectively.

As mentioned earlier, the sensing modules continually sample the current and voltage waveforms, and the detection algorithm examines the acquired data for probable faults according to the flowchart shown in Figure 3. Table 2 depicts the normalized values of energy and standard deviation of the γ -components of current and voltage waveforms associated with various sensing modules before and after a three-phase fault occurs at location *F1* in Figure 6. A study of the results shown in this table indicates that a fault has occurred in the microgrid. This is confirmed by noticing that following the occurrence of the fault, the normalized values of energy and standard deviation of both current and voltage waveforms associated with sensing modules 1, 2, 3, 4, 5, 9, 10 become greater than their respective thresholds.

After detecting the fault, the location algorithm uses the energy values of the γ - and α -components of current waveforms at sensing modules $m = 1, 2, 3, 4, 5, 9, 10$ (i.e., the

Module number (m)	$\overline{E}_{v,\gamma}^m$		$\overline{STD}_{v,\gamma}^m$		$\overline{E}_{i,\gamma}^m$		$\overline{STD}_{i,\gamma}^m$		Fault detected?
	Before	After	Before	After	Before	After	Before	After	
1	0.000216	0.058913	0.008123	0.058771	0.000047	0.029412	0.000134	0.012385	Yes
2	0.000166	0.085528	0.000132	0.17998	0.000007	0.03621	0.000061	0.031281	Yes
3	0.000917	0.305785	0.001092	0.408386	0.000169	0.08687	0.001083	0.053271	Yes
4	0.000773	0.203937	0.002313	0.284491	0.000174	0.056829	0.001336	0.049455	Yes
5	0.000751	0.075992	0.000496	0.132324	0.000207	0.033787	0.000178	0.017748	Yes
6	0.000486	0.006991	0.002742	0.004542*	0.000094	0.002655	0.000286	0.000695*	No
7	0.000427	0.001883	0.000628	0.001324*	0.000112	0.002216	0.000275	0.000435*	No
8	0.000044	0.010949	0.000354	0.005001*	0.000009	0.003645	0.000016	0.001337	No
9	0.000031	0.020076	0.000095	0.020902	0.000083	0.017477	0.000012	0.004522	Yes
10	0.000364	0.054799	0.002247	0.047169	0.000037	0.012452	0.000154	0.005611	Yes

TABLE 2. Values of $\overline{E}_{v,\gamma}^m$, $\overline{STD}_{v,\gamma}^m$, $\overline{E}_{i,\gamma}^m$, and $\overline{STD}_{i,\gamma}^m$ associated with various sensing modules before and after a three-phase fault at location *F1* in Figure 6. The asterisk sign (*) indicates that the corresponding quantity does not exceed its threshold value

Module number (m)	$\bar{E}_{i,\alpha}^m$	$\bar{E}_{i,\gamma}^m$	K_1^m
1	0.046301	0.029412	0.075713
2	0.134972	0.03621	0.171182
3	0.180342	0.08687	0.267211*
4	0.123007	0.056829	0.179836*
5	0.076605	0.033787	0.110392
9	0.013015	0.017477	0.030491
10	0.018518	0.012452	0.030971

TABLE 3. Values of $\bar{E}_{i,\alpha}^m$, $\bar{E}_{i,\gamma}^m$ and K_1^m associated with the sensing modules that detected a three-phase fault at location *F1* in *Figure 6*

modules that detected the fault) to determine their respective location indices K_1^m ($m = 1, 2, 3, 4, 5, 9, 10$). A study of the results shown *Table 3* indicates that the values of K_1^m at sensing modules $m = 3$ and 4 are greater than the other ones; in other words, the detection algorithm has correctly detected the fault on Line 2.

To determine the type of the fault, the characterization algorithm focuses on sensing module 3 (*i.e.*, the module with the maximum detection index, K_1^3). It uses the normalized energy values of the γ -components of the current ($\bar{E}_{i,\gamma}^3 = 0.08687$) and voltage waveforms ($\bar{E}_{v,\gamma}^3 = 0.305785$) to compute the characterization index $K_2^3 = 0.392655$. Referring to inequalities (13), it comes out that the occurred fault type is three-phase. In other words, the proposed method has succeeded to correctly detect a three-phase fault on Line 2.

3.2. Detection of an Asymmetric Fault

In order to attest the efficiency of the proposed method in detection of probable asymmetric faults in FREEDM microgrid, it is supposed that a double-phase-to-ground fault *F2* with fault resistance of 150 ohms on *a* and *b* phases of Line

5 in the main ring of the sample microgrid shown in *Figure 3* occurs. *Table 4* depicts the normalized values of energy and standard deviation of the γ -components of current and voltage waveforms associated with various sensing modules before and after a double-phase-to-ground fault occurs at location *F2* in *Figure 6*. A study of the results shown in this table indicates that a fault has occurred in the microgrid. This is confirmed by noticing that following the occurrence of the fault, the normalized values of energy and standard deviation of both current and voltage waveforms associated with sensing modules 1, 6, 7, 8, 9, 10 become greater than their respective thresholds.

Following the detection of the fault, the location algorithm uses the energy values of the γ - and α -components of current waveforms at the sensing modules that detected the fault to determine their location indices (*i.e.*, K_1^m ; $m = 1, 6, 7, 8, 9, 10$). From the results shown in *Table 5*, it is observed that the values of K_1^m at sensing modules $m = 9$ and 10 are greater than the other ones, indicating that the fault location has been correctly found on Line 5.

To determine the type of fault, the characterization algorithm focuses on sensing module 10 (*i.e.*, the module with the maximum detection index, K_1^{10}). (It uses the normalized energy values of the α -, β -, and γ -components of the current and voltage waveforms ($\bar{E}_{i,\alpha}^{10} = 0.617306$, $\bar{E}_{i,\beta}^{10} = 0.17395$, $\bar{E}_{i,\gamma}^{10} = 0.878141$, $\bar{E}_{v,\alpha}^{10} = 0.769943$, $\bar{E}_{v,\beta}^{10} = 0.731384$, and $\bar{E}_{v,\gamma}^{10} = 0.730141$) to compute the characterization indexes ($K_2^{10} = 1.608282$ and $K_3^{10} = 1.387248$). Referring to inequalities (13), it comes out that the proposed method has succeeded to correctly detect the double-phase-to-ground fault on Line 2. Besides phases *a* and *b* are involved in the fault as the values of $\bar{E}_{i,a}^{10} = 1.495447$ and $\bar{E}_{i,b}^{10} = 0.719955$ are greater than the value of $\bar{E}_{i,c}^{10} = 0.419021$.

Module number (m)	$\bar{E}_{v,\gamma}^m$		$\overline{STD}_{v,\gamma}^m$		$\bar{E}_{i,\gamma}^m$		$\overline{STD}_{i,\gamma}^m$		Fault detected?
	Before	After	Before	After	Before	After	Before	After	
1	0.000216	0.417062	0.008123	0.216847	0.000047	0.73293	0.000134	0.478596	Yes
2	0.000166	0.139366	0.000132	0.004895*	0.000007	0.193818	0.000061	0.008133	No
3	0.000917	0.065038	0.001092	0.003668*	0.000169	0.136925	0.001083	0.001655	No
4	0.000773	0.01278	0.002313	0.002471*	0.000174	0.096959	0.001336	0.001067*	No
5	0.000751	0.009862	0.000496	0.001521*	0.000207	0.076335	0.000178	0.00049*	No
6	0.000486	0.113955	0.002742	0.023083	0.000094	0.320739	0.000286	0.031277	Yes
7	0.000427	0.216547	0.000628	0.066619	0.000112	0.399256	0.000275	0.080545	Yes
8	0.000044	0.358353	0.000354	0.144565	0.000009	0.548812	0.000016	0.271525	Yes
9	0.000031	0.582577	0.000095	0.410413	0.000083	0.813669	0.000012	0.685018	Yes
10	0.000364	0.730141	0.002247	0.580231	0.000037	0.878141	0.000154	0.815025	Yes

TABLE 4. Values of $\bar{E}_{v,\gamma}^m$, $\overline{STD}_{v,\gamma}^m$, $\bar{E}_{i,\gamma}^m$, and $\overline{STD}_{i,\gamma}^m$ associated with various sensing modules before and after a double-phase-to-ground fault at location *F2* in *Figure 6*. The asterisk sign (*) indicates that the corresponding quantity does not exceed its threshold value

Module number (m)	$\bar{E}_{i,\alpha}^m$	$\bar{E}_{i,\gamma}^m$	K_1^m
1	0.389909	0.73293	1.122838
6	0.093202	0.320739	0.413941
7	0.300081	0.399256	0.699337
8	0.223274	0.548812	0.772086
9	0.492546	0.813669	1.306216*
10	0.617306	0.878141	1.495447*

TABLE 5. Values of $\bar{E}_{i,\alpha}^m$, $\bar{E}_{i,\gamma}^m$ and K_1^m associated with the sensing modules that detected a double-phase-to-ground fault at location F2 in Figure 6

3.3. Faults versus Switching Transients

To evaluate the reliability of the proposed method in cases where the microgrid encounters switching transients, we consider two switching scenarios in the FREEDM micrgrid shown in Figure 6. In the first scenario (Case A), a 200-kW DG source in the secondary of SST4 is switched on, whereas in the second scenario (Case B) a 300-kW load in the secondary of SST2 is switched off.

Values of the normalized energy and standard deviation of the γ -component of current and voltage waveforms associated with various sensing modules in Cases A and B are listed in Tables 6 and 7, respectively. A comparison of the results in these tables demonstrates that none of the two cases is considered to be a faulty case, although in rare cases the γ -component of current waveforms exceed their threshold values.

It is worth noting that the high-frequency isolation in a SST strongly decouples its two sides such that transient signals in either side are considerably attenuated in the opposite side [17, 18]. In fact, a sudden change in the power generation/consumption in a FREEDM microgrid leads to almost equal transients in the current waveforms of the three phases. As a result, the energy contents of current and voltage waveforms are much less than those observed in the case of a short-circuit fault. This is more accentuated when considering the standard deviations of the respective energy matrices.

Module number (m)	$10^6 \times \bar{E}_{v,\gamma}^m$	$10^6 \times \overline{STD}_{v,\gamma}^m$	$10^6 \times \bar{E}_{i,\gamma}^m$	$10^6 \times \overline{STD}_{i,\gamma}^m$	Fault detected?
1	3.1	22.7	30.6	16.2	No
2	85.2	67.1	212.1	176.2	No
3	277.6	79.4	361.2	280.4	No
4	525.4	83.8	497.5*	332.5	No
5	742.9	96.8	522.3*	403.8	No
6	185.1	65.8	335.4	272.4	No
7	29.5	57.5	120.3	152.2	No
8	6.2	39.5	84	132.2	No
9	4.6	31.2	38	60.1	No
10	1.9	0.6	9	12.1	No

TABLE 6. Values of $10^6 \times \bar{E}_{v,\gamma}^m$, $10^6 \times \overline{STD}_{v,\gamma}^m$, $10^6 \times \bar{E}_{i,\gamma}^m$, and $10^6 \times \overline{STD}_{i,\gamma}^m$ associated with various sensing modules in case A where the DG source in the secondary of SST4 is switched on in Figure 6. The asterisk sign (*) indicates that the corresponding quantity exceeds its threshold value

Module number (m)	$10^6 \times \bar{E}_{v,\gamma}^m$	$10^6 \times \overline{STD}_{v,\gamma}^m$	$10^6 \times \bar{E}_{i,\gamma}^m$	$10^6 \times \overline{STD}_{i,\gamma}^m$	Fault detected?
1	1143.4	2124.4	257.6	245.3	No
2	1633.5	3540.6	538.2*	335.5	No
3	1470.2	3186.6	368.7	317.3	No
4	1306.8	2832.5	438.6	304.6	No
5	980.1	2478.4	146.1	270.4	No
6	163.3	354	0.6	12.7	No
7	326.7	708.1	0.8	84.6	No
8	490	1062.2	4.3	109	No
9	816.7	1416.2	43.3	166.1	No
10	653.4	1770.3	16.8	216.2	No

TABLE 7 Values of $10^6 \times \bar{E}_{v,\gamma}^m$, $10^6 \times \overline{STD}_{v,\gamma}^m$, $10^6 \times \bar{E}_{i,\gamma}^m$, and $10^6 \times \overline{STD}_{i,\gamma}^m$ associated with various sensing modules in Case B where the load disconnected from the secondary of SST2 in Figure 6. The asterisk sign (*) indicates that the corresponding quantity exceeds its threshold value

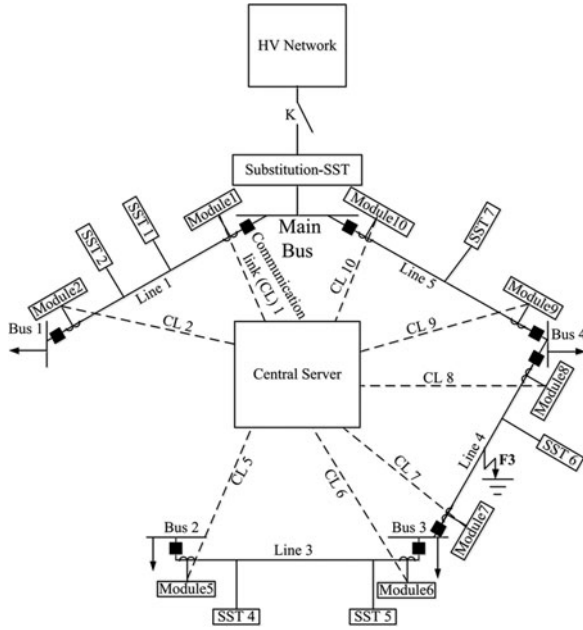


FIGURE 7. A topology of the studied FREEDM microgrid.

3.4. Radial Topology

To further examine the performance of the proposed method, we study the case where the FREEDM microgrid has a radial topology. Referring to Figure 6, we assume that Line 2 is disconnected while the DG sources in the secondary sides of SST4 and SST6, and the load in the secondary side of SST2 are switched off. In the new network (Figure 7) with radial topology, we assume a single-phase fault F3 with fault resistance of 150 ohms occurring on phase c of Line 4.

Table 8 depicts the normalized values of energy and standard deviation of the γ -components of current and voltage waveforms associated with various sensing modules before

Module number (m)	$\bar{E}_{v,\gamma}^m$		$\overline{STD}_{v,\gamma}^m$		$\bar{E}_{i,\gamma}^m$		$\overline{STD}_{i,\gamma}^m$		Fault detected?
	Before	After	Before	After	Before	After	Before	After	
1	0.000032	0.024992	0.000096	0.005209*	0.000007	0.136925	0.000012	0.001655	No
2	0.000355	0.004911	0.00164	0.003507*	0.000082	0.096959	0.0002	0.001067*	No
5	0.000548	0.001995*	0.001688	0.00216*	0.000123	0.076335	0.000209	0.00049*	No
6	0.000317	0.174746	0.000797	0.094599	0.000069	0.399256	0.00013	0.080545	Yes
7	0.000266	0.336555	0.000458	0.307923	0.000061	0.73293	0.000112	0.478596	Yes
8	0.000158	0.289179	0.000362	0.205282	0.000034	0.548812	0.000098	0.271525	Yes
9	0.000121	0.053554	0.000258	0.032778	0.000027	0.320739	0.000044	0.031277	Yes
10	0.000023	0.043789	0.000069	0.006951	0.000005	0.193818	0.000008	0.008133	Yes

TABLE 8. Values of $\bar{E}_{v,\gamma}^m$, $\overline{STD}_{v,\gamma}^m$, $\bar{E}_{i,\gamma}^m$, and $\overline{STD}_{i,\gamma}^m$ associated with various sensing modules before and after a single-phase fault at location F3 in Figure 7. The asterisk sign (*) indicates that the corresponding quantity does not exceed its threshold value

Module number (m)	$\bar{E}_{i,\alpha}^m$	$\bar{E}_{i,\gamma}^m$	K_1^m
6	0.100353	0.399256	0.499609
7	0.236248	0.73293	0.969178*
8	0.176813	0.548812	0.725625*
9	0.161139	0.320739	0.481878
10	0.060654	0.193818	0.254472

TABLE 9. Values of $\bar{E}_{i,\alpha}^m$, $\bar{E}_{i,\gamma}^m$, and K_1^m associated with the sensing modules that detected a single-phase fault at location F3 in Figure 7

and after a single-phase fault occurs. A study of the results shown in this table indicates that a fault has occurred in the microgrid. This is confirmed by noticing that following the occurrence of the fault, the normalized values of energy and standard deviation of γ -components of both current and voltage waveforms associated with sensing modules 6, 7, 8, 9, 10 become greater than their respective thresholds ($\bar{E}_{i,\gamma}^{TH} = 0.000449$, $\overline{STD}_{i,\gamma}^{TH} = 0.001078$, $\bar{E}_{v,\gamma}^{TH} = 0.002129$, and $\overline{STD}_{v,\gamma}^{TH} = 0.006575$).

Having detected the fault, the location algorithm uses the energy values of the γ - and α -components of current waveforms at the detecting sensing modules to determine K_1^m ($m = 6, 7, 8, 9, 10$). Computed values of K_1^m together with the respective normalized energy values of the γ - and α -components of current waveforms are presented in Table 9. From the results shown in this table, it is observed that the values of K_1^m at the sensing modules 7 and 8 are greater than the other ones, indicating that the fault location has been correctly detected on Line 4.

To determine the fault type and involved phases, the normalized energy values of the α -, β -, and γ -components of current and voltage waveforms at the sensing module 7 (i.e., the module with the maximum detection index) are used according to the fault characterization algorithm (Figure 5); it follows that $\bar{E}_{i,\gamma}^7 = 0.73293$, $\bar{E}_{v,\gamma}^7 = 0.396555$,

$\bar{E}_{i,\alpha}^m = 0.236248$, $\bar{E}_{v,\alpha}^m = 0.346272$, $\bar{E}_{i,\beta}^m = 0.256526$, $\bar{E}_{v,\beta}^m = 0.293451$, $K_2^7 = 1.129485$, and $K_3^7 = 0.582519$. Knowing that $K_{2\min} = 0.1$, $K_{2\max} = 1$, and $K_{3\min} = 1$ the use of inequalities (13) indicates that the fault type is single-phase. Besides, phase c is involved in the fault as the value $\bar{E}_{i,c}^7 = 0.836701$ is greater than the values of $\bar{E}_{i,a}^7 = 0.392911$ and $\bar{E}_{i,b}^7 = 0.484589$.

4. CONCLUSIONS

A method has been proposed to reliably detect, locate, and characterize various faults in a FREEDM microgrid. The proposed method uses the values of energy and standard deviation of voltage and current waveforms of the sensing modules deployed at the two ends of various branches within the microgrid. The proposed method makes use of the ST to obtain the characteristics of three-phase current and voltage waveforms and their Clarke components at different points in the network. The main feature of the proposed method is its capability to operate in a dynamic microgrid with varying topology. The performance of the proposed method has been demonstrated by applying it to a sample FREEDM microgrid with ring and radial structures. It has been shown that the proposed method is well capable of detecting, locating, and characterizing symmetric and asymmetric faults while being able to differentiate between short-circuit faults and switching transients due to variations in the network topology.

REFERENCES

- [1] Tiefu, Z Jie, Z, Bhattacharya, S., Baran, and Huang, A. Q., "An average model of solid state transformer for dynamic system simulation", *IEEE Power Energy Soc. Gen. Meet.*, pp. 1–8, 2009.
- [2] Xu, S., Huang, A. Q., and Burgos, R., "Review of solid-state transformer technologies and their application in power distribution systems", *IEEE J. Emerg. Select. Top. Power Electron.*, Vol. 1, pp. 186–198, 2013.
- [3] Tatcho, P., Hui, L., Yu, J., and Li, Q., "A novel hierarchical section protection based on the solid state transformer for the future renewable electric energy delivery and management (FREEDM) system", *IEEE Trans. Smart Grid*, Vol. 4, pp. 1096–1104, 2013.
- [4] Che, L., Khodayar, M., and Shahidepour, M., "Adaptive protection system for microgrids: protection practices of a functional microgrid system", *IEEE Electr. Mag.*, Vol. 2, pp. 66–80, 2014.
- [5] Hosseini, S. A., Abyaneh, H. A., Sadeghi, S. H. H., Razavi, F., and Nasiri, A., "An overview of microgrid protection methods and the factors involved", *Renew. Sust. Energy Rev.*, Vol. 64, pp. 174–186, 2016.
- [6] Al-Nasseri, H., Redfern, M. A., and Li, F., "A voltage based protection for micro-grids containing power electronic converters", *IEEE Power Energy Soc. Gen. Meet.*, 2006.
- [7] Al-Nasseri, H., Redfern, M. A., and O’Gorman, R., "Protecting micro-grid systems containing solid-state converter generation", *Int. Conf. Fut. Power Syst.*, 2005.
- [8] Brahma, S. M., "Fault location in power distribution system with penetration of distributed generation", *IEEE Trans. Power Deliv.*, Vol. 26, pp. 1545–1553, 2011.
- [9] Mishra, D. P., Samantaray, S. R., and Joos, G., "A combined wavelet and data-mining based intelligent protection scheme for microgrid", *IEEE Trans. Smart Grid*, Vol. PP, pp. 1–10, 2015.
- [10] Samantaray, S. R., Joos, G., and Kamwa, I., "Differential energy based microgrid protection against fault conditions", *IEEE PES Innov. Smart Grid Technol. (ISGT)*, pp. 1–7, 2012.
- [11] Petit, M., Le Pivert, X., and Garcia-Santander, L., "Directional relays without voltage sensors for distribution networks with distributed generation: use of symmetrical components", *Electr. Power Syst. Res.*, Vol. 80, pp. 1222–1228, 2010.
- [12] Sortomme, E., Venkata, S. S., and Mitra, J., "Microgrid protection using communication-assisted digital relays", *IEEE Trans. Power Deliv.*, Vol. 25, pp. 2789–2796, 2010.
- [13] Zeineldin, H., El-Saadany, E. F., and Salama, M. M. A., "Distributed generation micro-grid operation: control and protection", *Advanced Metering, Protection, Control, Communication, and Distributed Resources in Power Systems Conference*, pp. 105–111, 2006.
- [14] Dewadasa, M., Ghosh, A., and Ledwich, G., "Protection of microgrids using differential relays", *21 st Australasian Universities Power Engineering Conference (AUPEC)*, pp. 1–6, 2011.
- [15] Prasai, A., Yi, D., Paquette, A., Buck, E., Harley, R., and Divan, D., "Protection of meshed microgrids with communication overlay", *IEEE Energy Convers. Congr. Expos. (ECCE)*, pp. 64–71, 2010.
- [16] Pandeji, D. M., and Pandya, H. S., "Directional, differential and back-up protection of microgrid", *International Conference on Electrical, Electronics, Signals, Communication and Optimization (EESCO)*, pp. 1–5, 2015.
- [17] Huang, A. Q., Crow, M. L., Heydt, G. T., Zheng, J. P., and Dale, S. J., "The future renewable electric energy delivery and management (FREEDM) system: The Energy Internet", *IEEE Proc.*, Vol. 99, pp. 133–148, 2011.
- [18] Karady, G. G., and Xing, L., "Fault management and protection of FREEDM systems", *IEEE Power Energy Soc. Gen. Meet.*, pp. 1–4, 2010.
- [19] Xing, L., Thirumalai, A., and GKarady, G. G., "Design and development of an ultra fast pilot protection", *IEEE Power Syst. Conf. Expos. (PSCE)*, pp. 1–7, 2011.
- [20] Tatcho, P., Jiang, Y., and Li, H., "A novel line section protection for the FREEDM system based on the solid state transformer", *IEEE Power Energy Soc. Gen. Meet.*, pp. 1–8, 2011.
- [21] Pinnegar, C. R., and Mansinha, L., "Time-local fourier analysis with a scalable, phase-modulated analyzing function: the S-

transform with a complex window”, *Signal Process.*, Vol. 84, pp. 1167–1176, 2004.

- [22] Terzija, V., Valverde, G., Deyu, C., Regulski, P., Madani, V., Fitch, J., Skok, S., Begovic, M. M., and Phadke, A., “Wide-area monitoring, protection, and control of future electric power networks”, *IEEE Proc.*, Vol. 99, pp. 80–93, 2011.
- [23] El-Zonkoly, A. M. “Fault diagnosis in distribution networks with distributed generation”, *Electr. Power Syst. Res.*, Vol. 81, pp. 1482–1490, 2011.
- [24] Ray, P. K., Mohanty, S. R., and Kishor, N. “Disturbance detection in grid-connected distributed generation system using wavelet and S-transform”, *Electr. Power Syst. Res.*, Vol. 81, pp. 805–819, 2011.

BIOGRAPHIES

Reza Eslami received his B.S. and M.S. degrees in electrical engineering from Amirkabir University of technology in 2010 and 2012, respectively, where he is working toward a Ph.D. degree in power engineering. His research is focused on the operation and protection of distribution systems, including microgrids.

Seyed Hossein Hesamedin Sadeghi received his B.S. degree in electrical engineering from Sharif University of Technology, Tehran, Iran, in 1980, M.S. degree in power engineering from the University of Manchester Institute of Science and Technology, Manchester, U.K., in 1984, and Ph.D. degree in electronic systems engineering from the University of Essex, Colchester, U.K., in 1991. He is currently a Professor of electrical engineering with Amirkabir University of Technology, Tehran, Iran. Professor Sadeghi is a Senior Member of the IEEE. He is a holder of four patents and is the author/coauthor of one book, one book chapter, and more than 350 scientific papers published in reviewed journals and presented at international conferences. His current research

interests include power system protection and electromagnetic compatibility.

Hossein Askarian-Abyaneh received his B.S. degree from Iran University of Science and Technology in 1976 and M.S. degree from Tehran University, Tehran, Iran, in 1982, both in electrical engineering. He received a second M.S. degree and the Ph.D. degree, both in power engineering, from the University of Manchester Institute of Science and Technology, Manchester, U.K., in 1985 and 1988, respectively. Currently, he is a Professor with the Department of Electrical Engineering, Amirkabir University of Technology, Tehran, Iran. He has published numerous scientific papers in reviewed journals and presented at international conferences. His research interests include power system protection and power quality.

Adel Nasiri received his B.S. and M.S. degrees from Sharif University of Technology, Tehran, Iran, in 1996 and 1998, respectively, and PhD degree from the Illinois Institute of Technology, Chicago, Illinois, in 2004, all in electrical engineering. He is presently the Associate Dean for Research in the College of Engineering & Applied Science and Director, Center for Sustainable Electrical Energy Systems in the Department of Electrical Engineering and Computer Science at the University of Wisconsin–Milwaukee. Professor Nasiri is a Senior Member of the IEEE and is currently an Editor of IEEE Transactions on Smart Grid, Associate Editor of IEEE Transactions on Industry Applications, an Editor of Power Components and Systems, and Associate Editor of the International Journal of Power Electronics. He was the general Chair of 2012 IEEE SLED Symposium, ICRERA 2014, and IEEE PEMWA 2014. His research interests include renewable energy interface, energy storage, and microgrids.